

*Short Note*

## Validation of Regional Travel-Time Predictions along the Tethyan Margin for Three *P*-Velocity Models Built with Different Approaches

by Sung-Joon Chang, Suzan Van der Lee, and Megan P. Flanagan

**Abstract** We validate the performance of three *P*-velocity models built with different approaches on regional travel-time prediction for the Tethyan margin in order to test how well they predict independently observed travel times. The three models are constructed with travel-time tomography, a compilation of *a priori* geologic and geophysical information, and empirical scaling with adjustment from *P*-arrival inversion, respectively. We compared the synthetics with reference travel times (ground truth data) obtained by using events or explosions located within 25 km with 95% confidence. We found variance of travel times is not an adequate tool to assess the performance of velocity models, because predicted travel times that have small variance can have very different mean value from that of observed ones. Therefore, we propose an alternative way, variance estimation with mean of observed travel times (zero mean). This technique is more efficient to assess the mismatch between synthetics and observed travel times. Among the three models we investigated, the EAPV11 model built mainly with the empirical scaling shows better performance on the travel-time prediction. This result is intriguing, because this model inherits crustal velocity structure, Moho depth, *Pn* velocities, and upper-mantle structure that affects travel times at regional distance, mostly from a scaled 3D *S*-velocity model for the same region. This fact may imply that although errors may be included in this scaling, this way would work better than conventional *P*-arrival inversion. This difference likely exists because surface waves have a better lateral resolution for the crust and uppermost mantle than travel times.

*Online Material:* Histograms of travel-time residuals and correction surfaces of travel times with respect to *iasp91* for 33 stations.

### Introduction

Accurate crustal and uppermost mantle velocity models are utilized in and needed for various subjects, such as location of events and explosions, source mechanism determination, event yield estimation, ground motion, predictions from scenario earthquakes, etc. The nuclear tests by North Korea in 2006, 2009, and 2013 have highlighted the need for such models, especially for the estimation of first-arriving *P* travel times at regional distances, which are critical for the ability to locate small earthquakes or small-yield nuclear tests. Many 3D regional and global seismic velocity models exist, derived mainly through seismic tomography. However, travel times at regional distance are hard to predict due to following reasons. First, travel times at regional distance are greatly sensitive to complex heterogeneity in crustal and uppermost

mantle velocity structure. Second, it is hard to acquire a good lateral resolution for shallow depth ranges with travel-time data due to their steep incident angles at the depth. Furthermore, in aseismic regions with few stations, few travel-time data can be obtained, which results in poor *P*-velocity models. These facts may cast doubts to the efficiency of *P*-velocity models built with tomographic techniques in estimating travel times at regional distance, so it is necessary to consider *P*-velocity models constructed from a variety of methodologies. For the comparison between models, we should find a way to quantitatively assess the performance of various *P*-velocity models for the travel-time prediction. For this purpose, we need to test each model against independent observations.

We select three  $P$ -velocity models for the Tethyan margin that are derived from three different approaches. The Tethyan margin is mixed with active orogenic belts and aseismic regions, so it is a good example to test the potential performance of velocity models for predicting accurate arrival times. The first model is a global  $P$ -velocity model by Bijwaard *et al.* (1998), which is constructed with  $P$ -arrival inversion. This model is complemented by CRUST2.0 (Bassin *et al.*, 2000) for fine crustal structure. The second is derived from compilation of *a priori* information by Pasyanos *et al.* (2004). The last model is estimated using empirical scaling relationships between  $P$ - and  $S$ -velocity models and adjustment with  $P$ -arrival inversion (Chang *et al.*, 2012).

Synthetic arrival times are calculated for each model with a finite-difference code and compared with independent observations collected by Ruppert *et al.* (2005), which have location uncertainties as small as 25 km with 95% confidence.

### Velocity Models

The first model we validate is derived from the tomographic inversion of  $P$  arrivals (Bijwaard *et al.*, 1998). Although this model is a global model, it improves the resolution along the Tethyan margin by adopting the reprocessed global data set of Engdahl *et al.* (1998) and utilizing phases such as  $pP$  and  $pwP$ , as well as direct  $P$  phases. Through adaptive parameterization, cells as small as  $0.6^\circ$  were used for the crust and the upper mantle in regions densely covered by wavepaths. As a global model, this model does not include Moho variations and fine crustal structure. We add CRUST2.0 (Bassin *et al.*, 2000) to the model of Bijwaard *et al.* (1998) to supplement crustal velocity structure and Moho variation and call this model BCRUST2.

The second is the *a priori* model WENA1.0 by Pasyanos *et al.* (2004). This model is derived from compilation of geologic and geophysical information, such as sediment thickness, crustal and upper-mantle velocity models, topography, receiver function measurements, surface-wave dispersions, and  $Pn$  velocity tomography. The model is mainly based on CRUST5.1 (Mooney *et al.*, 1998), the high-resolution  $1^\circ$  sedimentary layer of Laske and Masters (1997), and the 3SMAC mantle model of Nataf and Ricard (1996) with  $2^\circ$  resolution. For aseismic regions, extrapolation of properties of data-rich regions that share similar tectonic features and history is assumed. *A priori* models have advantages over tomographic models, such as even coverage for both active and inactive tectonic areas and the preservation of sharp features.

The third model is obtained by the combination of an empirical scaling relationship and  $P$ -arrival time inversion (EAPV11; Chang *et al.*, 2012). In other words, EAPV11 is estimated with regional and teleseismic  $P$  and  $PKP$  arrivals relative to a 3D reference model, which is obtained by scaling an  $S$ -velocity model for the same region. The 3D  $S$ -velocity model was estimated from the joint inversion

of teleseismic  $S$  arrivals, regional waveform fits, Rayleigh-wave group velocities, and Moho depth constraints (Chang *et al.*, 2010). Our scaling is empirical and based on observations of Schmid *et al.* (2004) of  $P$  and  $S$  delay times in the Mediterranean region, adjusted for the larger study region used here. EAPV11 is defined as

$$\mathbf{m}_\alpha = \mathbf{m}_\alpha^{\text{1D}} + \mathbf{m}_\alpha' + \mathbf{m}_\alpha'', \quad (1)$$

in which  $\mathbf{m}_\alpha^{\text{1D}}$  is the 1D reference  $P$ -velocity model *iasp91* (Kennett and Engdahl, 1991),  $\mathbf{m}_\alpha'$  represents the 3D  $P$  perturbations from the scaled  $S$ -velocity model of Chang *et al.* (2010), and  $\mathbf{m}_\alpha''$  indicates the  $P$ -velocity anomalies from the inversion of residual delay times obtained by subtracting the predicted effects of  $\mathbf{m}_\alpha'$  and  $\mathbf{m}_\alpha^{\text{1D}}$  from original observed times. This approach allows us to retain information on aseismic regions and shallow depth ranges provided by regional  $S$  and surface waves, which is hardly constrained by  $P$ -arrival times. Thus, the crustal and uppermost mantle structure in EAPV11 that affects travel times at regional distances is mainly inherited from the 3D reference model. The Moho variation is also retained from the  $S$ -velocity model. This Moho variation is a part of  $\mathbf{m}_\alpha'$  and used to calculate predicted times, which is subtracted from the  $P$ -arrival times.

Crustal and mantle structure are inverted for simultaneously in constructing EAPV11. Because we use a 1D reference model, *iasp91*, with a 35 km Moho depth, there are cases in which the estimated Moho is shallower or deeper than 35 km. In these cases, we extend mantle reference velocity or crustal reference velocity to the estimated Moho to obtain reasonable travel times. However, velocities in these extended regions are partly compensated by the estimated anomalies in the inversion, so we reduced the strength of 3D perturbations for the extended regions. Trial and error showed that reducing the strength of these near-Moho anomalies by a factor of 2 positively affected the data fit. The distance between lateral grids of the model is approximately  $1^\circ$  at the surface, and anomalies at various depths are parameterized down to 1930 km vertically (Chang *et al.*, 2012).

Maps of  $P$  velocities at 25 km depth and  $Pn$  velocities from the three models are presented in Figure 1. We choose a range which spans  $0^\circ$  to  $60^\circ$  latitude and  $-20^\circ$  to  $75^\circ$  longitude, which is common for the three models. Although there are interesting small-scale differences, the maps of the three models at 25 km are largely consistent with one another. Overall, EAPV11 shows slightly higher velocity than the other two models. The maps of  $Pn$  velocities of the three models appear very different from one another. EAPV11 has relatively slow  $Pn$  velocities, especially beneath continents. BCRUST2 and WENA1.0 share similar  $Pn$  velocities, but WENA1.0 shows sharp boundaries beneath Turkey, Iran, western Arabia, East Africa, the Gulf of Aden, and the Carlsberg Ridge, which is possible in *a priori* models. The Moho variations used in the three models are presented in Figure 2. CRUST2.0 is used for BCRUST2, and CRUST5.1 is used for WENA1.0. EAPV11 has its own Moho variation.

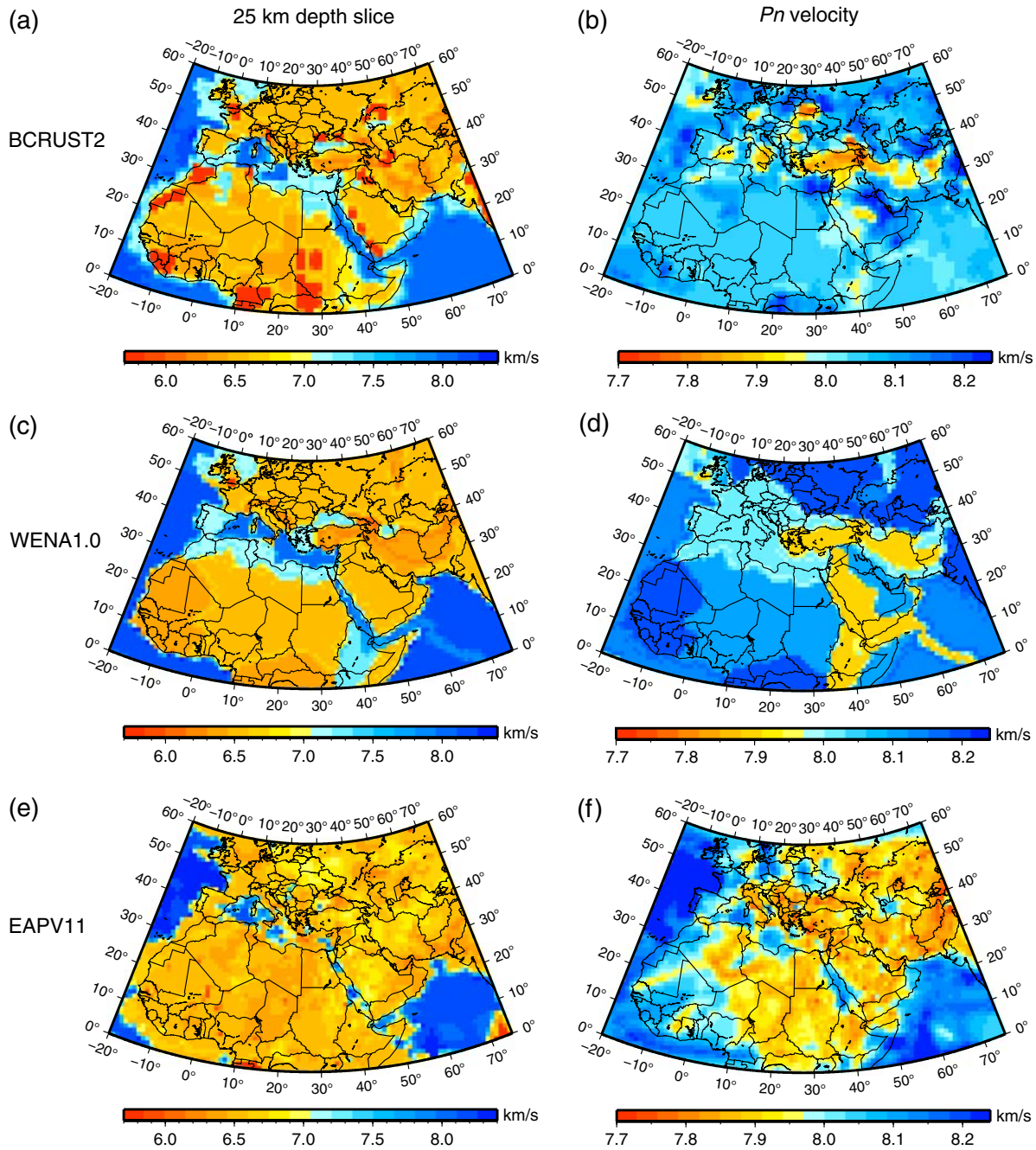


**Figure 1.** Twenty-five kilometer depth slices and  $P_n$  velocity distributions from (a–b) BCRUST2, (c–d) WENA1.0, and (e–f) EAPV11 models. The color version of this figure is available only in the electronic edition.

### Ground Truth Data and Method

To validate the accuracy of travel-time prediction through the three models, we would want to compare our predictions with travel-time observations from well-located events, that is, with ground truth (GT) data. We use a GT data set that meets the criteria of [Bondár \*et al.\* \(2004\)](#) and includes events or known-location sources, such as explosions, to provide accurate reference data. From the GT data, we selected 4525 travel times of first-arriving  $P_g$ ,  $P_n$ , and  $P$  phases at 33 stations up to epicentral distance of 50° to

evenly cover the study region shown in [Figure 3](#). Because we use all first-arriving phases out to epicentral distance of 50°, phase identification is hampered by  $P$  and  $P_n$  crossover, as well as  $P$  triplications from 410 to 660 km discontinuities. However, this approach will provide a realistic condition to assess the performances of the three  $P$ -velocity models for the regional recording of a moderate event or explosion. The uncertainty of the locations is at most 25 km with 95% confidence, and focal depth is less than 30 km. Details on the data are given in [Ruppert \*et al.\* \(2005\)](#) and [Flanagan \*et al.\* \(2007\)](#).

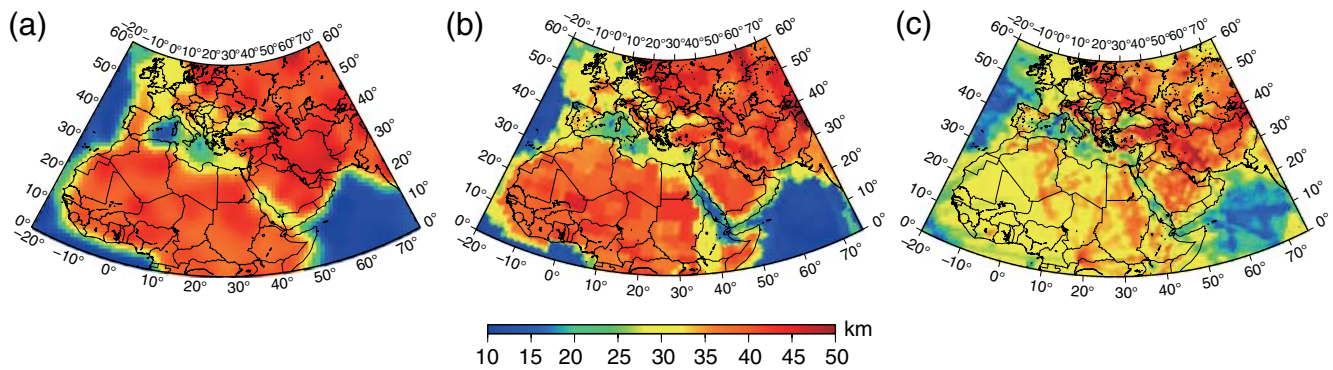


**Figure 2.** Three Moho variations used in testing the three  $P$ -velocity models: (a) CRUST5.1 (Mooney *et al.*, 1998), (b) CRUST2.0 (Bassin *et al.*, 2000), and (c) EAPV11 (Chang *et al.*, 2012). The color version of this figure is available only in the electronic edition.

One of our test models, WENA1.0, includes sharp horizontal and vertical gradients. This condition makes it difficult to calculate accurate ray paths and travel times. Although finite difference is computationally expensive, it can provide relatively accurate travel times in the presence of sharp gradients. Thus, we use the finite-difference (FD) code first developed by Vidale (1988, 1990) and refined by Hole and Zelt (1995) and Flanagan *et al.* (2007) later to properly calculate phases traveling along the spherical Earth with sharp boundaries. Grids are located with 5 km intervals in a Cartesian coordinate that includes the Earth in its grid box. This FD code generates first arriving  $P$ -travel times at every grid point. We calculate correction surfaces by subtracting 1D predicted travel times based on *iasp91* from predicted 3D travel times at each grid point. Further details on the FD code are given in Flanagan *et al.* (2007).

### Results and Discussion

We estimated travel-time predictions from the three models using the 3D FD code, subtracted these from observed GT travel times, and calculated traditional variance reduction at each station (VR in Table 1) via the following equation:

$$VR = \sum_i^n \frac{(\text{RES}_{iasp91_i} - \text{MEAN}_{iasp91})^2 - (\text{RES}_{mod_i} - \text{MEAN}_{mod})^2}{(\text{RES}_{iasp91_i} - \text{MEAN}_{iasp91})^2} \times 100, \quad (2)$$

in which  $\text{RES}_{iasp91_i}$  and  $\text{MEAN}_{iasp91}$  are the  $i$ th travel-time residual between observed and synthetic travel times from *iasp91* and the mean residual time for the residuals, respectively.  $\text{RES}_{mod_i}$  and  $\text{MEAN}_{mod}$  are the  $i$ th travel-time residual between observed and synthetic travel times from one of the 3D models and the mean residual time for the residuals, respectively.  $n$  is the total number of travel times for the station. Thus, VR measures variance reduction with respect to the variance with *iasp91*.

The three models show variance reduction for most stations, but with different patterns (Table 1). The BCRUST2

model shows large variance reduction at stations in orogenic belts such as BKR and TAB, whereas WENA1.0 and EAPV11 models predict travel times better at stations in boundary of continents such as ARO and TIC and in stable craton or shields such as RYD and SVE, respectively. There are also some stations like ELL, LKO, and TAM in which the three models show comparable variance reduction to one another. Only at station TCF all models show variance increase. Most events recorded at this station are located near Italy and Greece (E available in the electronic supplement to this article), in which velocity variation changes rapidly. However, the average of the velocity variation is approximately zero, which makes the 1D reference model well behaved. Average variance reductions of the values at 33 stations from BCRUST2 and EAPV11 are similar to 21.1% and 20.1%, respectively. However, the performance of WENA1.0 is behind the other two models, marking 15.3% of variance reduction.

To test our assumption that BCRUST2 is better able to predict  $P$ -arrival times than CRUST2.0 or the BSE model alone, we paired CRUST2.0 with *iasp91* velocities for the mantle and the BSE model with *iasp91* velocities for the crust. We predicted arrival times from these two simple model pairs and compared them to GT25 data, which reached 5.6% and

15.2% variance reductions, respectively. Both of these variance reductions are smaller than the 21.1% of variance reduction obtained with predictions from BCRUST2. We thus confirm that BCRUST2 is better than individual models for regional travel-time prediction, and the mantle model of Bijwaard *et al.* (1998) demonstrates more influence than CRUST2.0 on the variance reduction of BCRUST2.

Based on the variance reduction results, it seems BCRUST2 is the best model for travel-time predictions for the Tethyan margin. However, based on histograms at station MAIO in Figure 4 for example, BCRUST2 model achieves

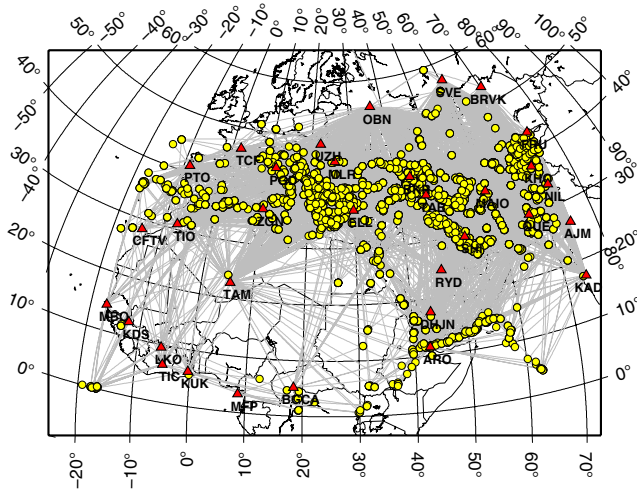


**Figure 3.** Wavepaths for the GT25 data set. Stations and events are indicated by triangles and circles, respectively. The color version of this figure is available only in the electronic edition.

more variance reduction than that from EAPV11 model although the histogram from BCRUST2 is biased to have a mean of  $-1.26$  s, which indicates most predicted travel times arrive later than observed ones. This bias is also shown in the correction surfaces of the BCRUST2 model and WENA1.0 (Fig. 4), which shows significant discrepancy between GT25 data and model-predicted times. Therefore, in order to represent the performance of the velocity models in terms of travel-time prediction, we need to take the mean into account in a new way, for example, by using variance estimation with respect to a fixed mean of 0 s (VR0 in Table 1), which represents coincidence between predicted and observed travel times via the equation,

$$VR0 = \sum_i^n \frac{(RESiasp91_i)^2 - (RESmod_i)^2}{(RESiasp91_i)^2} \times 100, \quad (3)$$

which is the same as equation (2) if we put zeros to the mean values. Thus, in VR0 each variance is measured with

**Table 1**  
Statistics of Travel-Time Predictions for All Stations from the GT25 Data Set

Station	Number of Data	Mean			VR* (%)			VR0† (%)		
		BCRUST2	WENA1.0	EAPV11	BCRUST2	WENA1.0	EAPV11	BCRUST2	WENA1.0	EAPV11
AJM	140	0.9673	-0.2493	-0.5255	-20.247	-2.365	15.235	-31.539	0.534	13.807
ARO	132	1.8051	1.2904	1.0092	15.035	44.954	23.045	-21.558	28.592	21.736
BGCA	19	-0.2502	0.0341	-0.5865	-11.976	-3.053	1.775	-9.615	1.317	-7.407
BKR	292	-0.4405	-0.8837	0.1911	33.026	24.374	17.339	58.195	43.106	51.905
BRVK	66	-2.0191	-1.6111	-1.1320	28.103	31.106	27.479	-20.543	10.090	33.687
CFTV	9	-2.9685	-1.0697	-1.7941	51.200	54.552	67.140	24.029	72.716	65.554
DHJN	72	0.6805	-0.8054	-0.4635	38.872	19.175	32.595	30.892	7.822	30.315
ELL	257	0.2093	-0.4387	0.1658	30.044	22.811	23.622	61.905	56.024	58.683
FRU	198	-0.3893	-0.3122	0.2577	51.066	9.012	54.098	56.860	24.672	61.543
KAD	80	0.0536	0.4580	0.5589	16.179	21.711	6.272	16.593	19.295	2.551
KDS	24	-1.2503	-0.0207	0.0038	46.411	54.181	50.608	52.975	74.375	72.381
KHO	183	-0.1838	-1.3900	-0.2782	47.576	18.077	39.155	52.866	-21.069	44.331
KUK	16	-1.2806	-0.2162	-0.6525	4.490	-24.300	-0.378	-55.147	1.487	1.229
LKO	13	-1.2554	0.0754	-0.2092	33.812	29.483	38.871	34.825	52.314	58.157
MAIO	173	-1.2563	-2.5191	-0.3725	52.452	33.769	41.329	15.625	-115.496	38.611
MBO	25	-1.4738	-0.2010	-0.4498	33.618	42.069	33.815	12.322	50.526	41.201
MFP	5	-1.6118	0.6042	-2.5178	-7.952	-53.982	4.658	-59.115	-11.785	-179.981
MLR	263	0.1095	0.2266	0.2655	4.333	-0.303	0.814	43.842	40.259	40.487
NIL	186	-0.4230	-0.3834	-0.3377	41.951	26.995	38.994	47.805	36.051	46.751
OBN	340	-1.8774	-0.6388	-0.4333	31.773	36.212	19.082	-3.146	59.710	55.308
PGD	113	0.4366	0.3159	-0.0440	15.537	-1.972	6.168	44.228	36.552	44.296
PTO	75	-0.4456	-0.1675	1.2624	32.136	25.306	18.883	34.001	31.693	-9.748
QUE	174	0.1340	-1.1446	0.5372	-13.757	-18.417	2.173	50.360	15.603	50.389
RYD	97	0.0288	-0.9225	-0.3864	16.265	1.860	30.061	17.382	-13.443	28.089
SHI	180	-0.6761	-2.3883	-0.5935	35.320	15.487	24.848	23.748	-129.240	15.941
SVE	174	-0.8953	-1.5599	-0.1109	35.271	21.867	38.914	21.323	-34.763	45.951
TAB	290	-0.1311	-0.4845	0.6034	23.656	10.390	6.515	63.726	54.542	50.800
TAM	141	-0.1843	-0.1717	-0.0839	19.284	16.702	11.263	18.610	16.155	11.337
TCF	215	-0.5111	-1.0506	0.2420	-20.341	-11.949	-42.639	-35.409	-94.823	-40.414
TIC	38	-0.6470	0.2888	0.1675	-9.660	16.549	-7.077	27.430	49.315	36.489
TIO	124	0.4318	0.6282	0.6017	13.920	11.196	3.132	12.383	0.453	-5.491
UZH	312	-0.4764	0.0563	0.2178	9.208	20.528	18.363	14.330	30.017	26.980
ZGN	99	-0.7735	0.0868	-1.0192	20.085	13.221	17.062	18.407	22.238	8.270
Average	4525	-0.5020	-0.4413	-0.1790	21.112	15.310	20.097	18.745	12.571	24.659

\*Variance reduction.

†Variance reduction with zero mean.

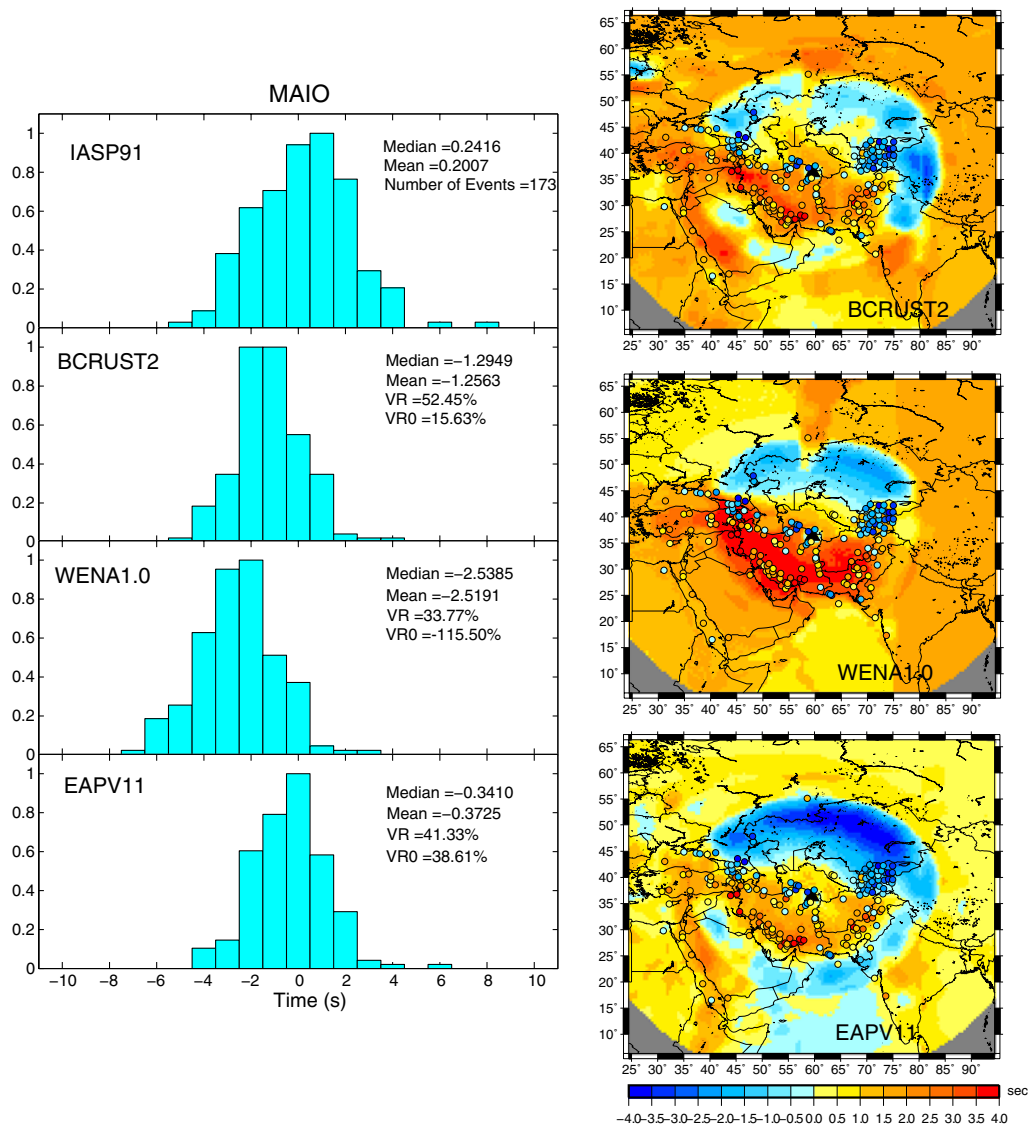


**Figure 4.** (Left) Histograms of travel-time residuals (GT25—predicted travel times) and (right) correction surfaces for the BCRUST2, WENA1.0, and EAPV11 models at station MAIO. The correction surfaces represent variations of travel times relative to *iasp91* at 10 km depth (model-predicted times—*iasp91*-predicted times) as seen by station MAIO (black triangle). Travel-time residuals between GT25 data set (< 30 km depth) and *iasp91* (GT25—*iasp91*-predicted times) are superposed on the correction surfaces as circles with the same scale as the correction surface. The color version of this figure is available only in the electronic edition.

zero mean, thereby indicating distribution from the zero residual.

When we calculate the variance estimation with zero mean at station MAIO, the performance of BCRUST2 decreases from 52.45% to 15.63%, whereas that of EAPV11 remains similar at variance reduction of 38.61% from 41.33%. These variance reductions with zero mean are consistent with correction surfaces (Fig. 4), where the best match between GT data and predicted travel times is obtained with EAPV11. Another example of station SVE (Fig. 5) also shows a better match between observed and synthetics with EAPV11 than with the other two models especially for Iran. The characteristics of the match between synthetics and observed travel times are well documented in the variance reductions with

zero mean. For 33 tested stations, EAPV11 shows the largest variance reduction with zero mean of 24.7%; this is superior to the other models, which show 18.7% and 12.6% (Table 1).

This good variance reduction with zero mean from EAPV11 is achieved although poor variance reduction of  $-179.98\%$  is observed at station MFP, which may be partly due to lack of data in the tomographic inversions. If we exclude station MFP, the average variance reduction with zero mean through EAPV11 improves to 31.5%, whereas further variance reduction by other models is only 1%–2%. Mean of EAPV11 is also improved from  $-0.1790$  to  $-0.1059$  when excluding station MFP.

Next, one might wonder whether the improvements provided by EAPV11 are caused by our use of the 3D reference

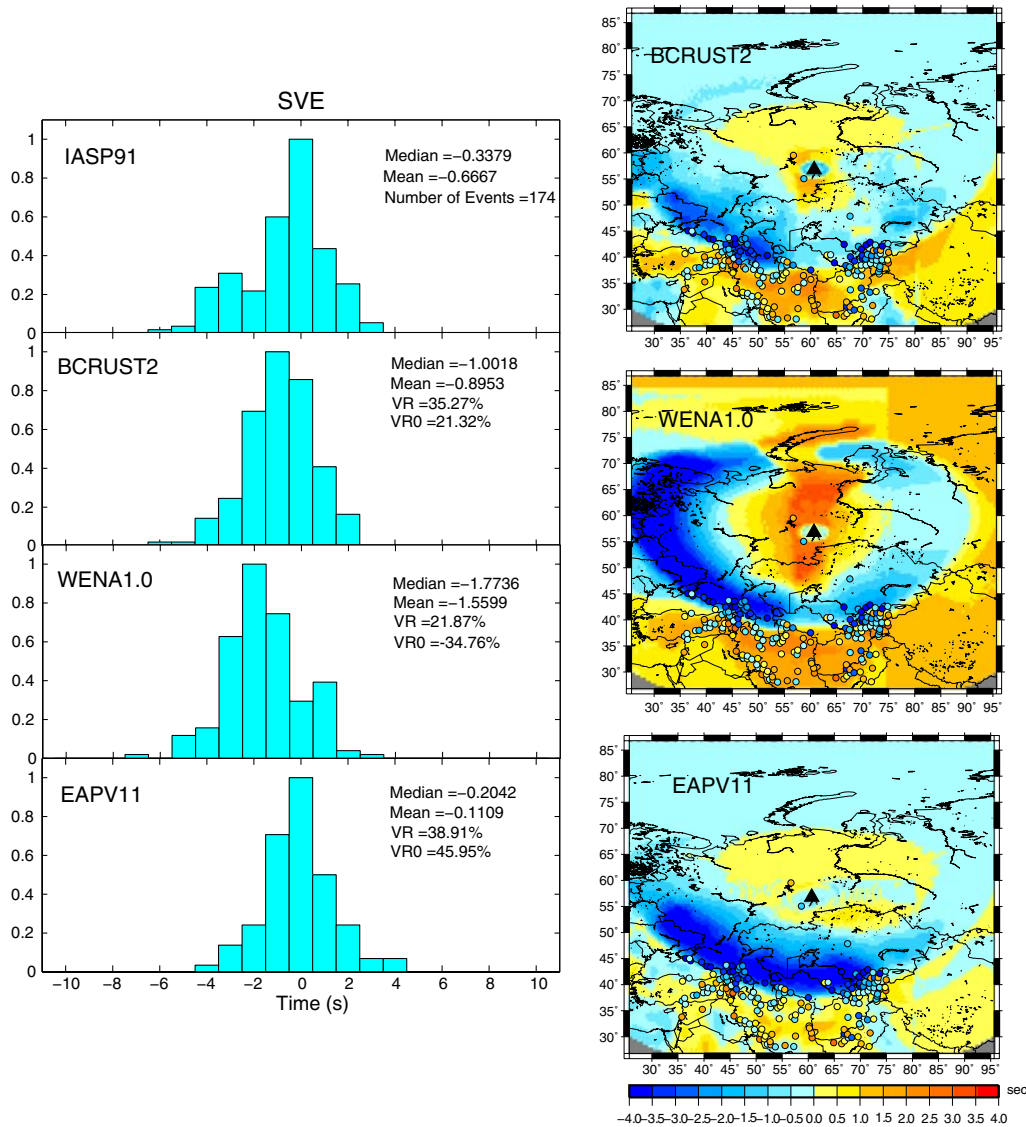


**Figure 5.** (Left) Histograms of travel-time residuals (GT25—predicted travel times) and (right) correction surfaces for the BCRUST2, WENA1.0, and EAPV11 models at station SVE. Other explanations are the same as in Figure 4. The color version of this figure is available only in the electronic edition.

model or by the used  $P$  arrivals spanning a longer time period than was available for the BCRUST2 model. To answer for this question, we inverted all  $P$  arrivals relative to the 1D reference model *iasp91*. We predicted  $P$  arrivals using this “ $P$ -arrival inversion only” model and compared them with GT25 data. The comparison shows a 5.9% of variance reduction with zero mean, which is much smaller than 24.7% of VR0 with EAPV11. On the other hand, we used the 3D reference model itself to predict  $P$  arrivals to be compared with GT25 data. That comparison shows 22.6% of VR0. This variance reduction with zero mean for the 3D reference model is larger than those obtained from BCRUST2 and WENA1.0. This demonstrated that the 3D reference model plays an essential role in the improved ability of EAPV11 to predict  $P$ -arrival times.

This result is intriguing because the crustal structure, Moho variation,  $P_n$  velocity, and the uppermost mantle of EAPV11, which most affect travel times at regional distance, are inherited from the 3D reference model, which is scaled from our 3D  $S$ -velocity model (Chang *et al.*, 2010). This may mean that even though scaling  $S$ -velocity model to  $P$ -velocity model inevitably contains some errors in the estimation of  $P$  velocities, this scaling is still effective to construct reliable regional  $P$ -velocity models, because surface waves have good sensitivity to shallow depth over travel times. The scaling relationship works well for the Tethyan margin, one of densely covered regions by events and stations, which is a good condition for seismic tomography. Thus, we expect the scaling would work much better for aseismic regions not well covered with  $P$  arrivals.

## Conclusions

We investigated the performance of three  $P$ -velocity models derived from different approaches on the travel-time predictions by comparing synthetic arrival times estimated with a 3D FD code with well-located observed GT25 data (Flanagan *et al.*, 2007). We found that traditional variance reduction does not entirely capture a model's performance, because it only cares for the distribution from the mean that can be far from the one of the observed travel times. Therefore, we propose an alternative way, variance reduction with zero mean for the assessment of velocity models on travel-time predictions. We found that this approach better reflects the information contained in the correction surfaces.

Based on the variance reduction with zero mean (VR0) at 33 stations along the Tethyan margin, EAPV11 shows better performance on predicting travel times fitted with observed ones than the other two models. This is an intriguing feature, because EAPV11 model mostly inherits the structures that dominate travel-time prediction at regional distances, such as crustal velocity,  $Pn$  velocity, Moho depth, and the uppermost mantle, from the 3D reference model obtained by scaling our 3D  $S$ -velocity model. Although some errors may be contained in the estimated  $P$  velocities, this approach may provide an alternative way to constrain structure of aseismic regions and shallow depth ranges, for which  $P$ -arrival data hardly can provide a good resolution. Correction surfaces and histograms for all stations  are available in the electronic supplement.

## Data and Resources

No data were used in this paper. All figures were created using the Generic Mapping Tools version 4.5.2 ([www.soest.hawaii.edu/gmt](http://www.soest.hawaii.edu/gmt), last accessed August 2013; Wessel and Smith, 1998).

## Acknowledgments

We thank Stewart Fishwick for critical and constructive comments, which greatly improved the manuscript. This study was supported by a 2013 Research Grant from Kangwon National University and the U.S. Department of Energy under Contract Number DE-FC52-04NA25541.

## References

- Bassin, C., G. Laske, and G. Masters (2000). The current limits of resolution for surface wave tomography in North America, *Eos Trans. AGU* **81**, F897.
- Bijwaard, H., W. Spakman, and E. R. Engdahl (1998). Closing the gap between regional and global travel time tomography, *J. Geophys. Res.* **103**, 30,055–30,078.
- Bondár, I., S. Myers, E. R. Engdahl, and E. Bergman (2004). Epicenter accuracy based on seismic network criteria, *Geophys. J. Int.* **156**, 483–496.
- Chang, S.-J., S. van der Lee, and M. P. Flanagan (2012). A new  $P$ -velocity model for the Tethyan margin from a scaled  $S$ -velocity model and the inversion of  $P$ - and  $PKP$ -delay times, *Phys. Earth Planet. In.* **210/211**, 1–7, doi: [10.1016/j.pepi.2012.08.005](https://doi.org/10.1016/j.pepi.2012.08.005).

- Chang, S.-J., S. van der Lee, M. P. Flanagan, H. Bedle, F. Marone, E. M. Matzel, M. E. Pasyanos, A. J. Rodgers, B. Romanowicz, and C. Schmid (2010). Joint inversion for 3-dimensional  $S$ -velocity mantle structure along the Tethyan margin, *J. Geophys. Res.* **115**, no. B08309, doi: [10.1029/2009JB007204](https://doi.org/10.1029/2009JB007204).
- Engdahl, E. R., R. Van der Hilst, and R. Buland (1998). Global teleseismic earthquake relocation with improved travel times and procedures for depth determination, *Bull. Seismol. Soc. Am.* **88**, 722–743.
- Flanagan, M. P., S. C. Myers, and K. D. Koper (2007). Regional travel-time uncertainty and seismic location improvement using a three-dimensional a priori velocity model, *Bull. Seismol. Soc. Am.* **97**, 804–825.
- Hole, J. A., and B. C. Zelt (1995). 3D finite difference reflection travel times, *Geophys. J. Int.* **121**, 427–434.
- Kennett, B. L. N., and E. R. Engdahl (1991). Traveltimes for global earthquake location and phase identification, *Geophys. J. Int.* **105**, 429–465.
- Laske, G., and T. G. Masters (1997). A global digital map of sediment thickness, *Eos Trans. AGU* **78**, F483.
- Mooney, W. D., G. Laske, and T. G. Masters (1998). CRUST5.1: A global crustal model at  $5^\circ \times 5^\circ$ , *J. Geophys. Res.* **103**, 727–747.
- Nataf, H.-C., and Y. Ricard (1996). 3SMAC: An a priori tomographic model of the upper mantle based on geophysical modeling, *Phys. Earth Planet. In.* **95**, 101–122.
- Pasyanos, M. E., W. R. Walter, M. P. Flanagan, P. Goldstein, and J. Bhattacharyya (2004). Building and testing an a priori geophysical model for western Eurasia and North Africa, *Pure Appl. Geophys.* **161**, 235–281.
- Ruppert, S., D. Dodge, A. Elliott, M. Ganzberger, T. Hauk, and E. Matzel (2005). Enhancing seismic calibration research through software automation and scientific information management, in *Proc. of the 27th Seismic Research Review: Ground-Based Nuclear Explosion Monitoring Technologies*, Rancho Mirage, California, 20–22 September 2005, 937–945.
- Schmid, C., S. van der Lee, and D. Giardini (2004). Delay times and shear wave splitting in the Mediterranean region, *Geophys. J. Int.* **159**, 275–290.
- Vidale, J. (1988). Finite-difference calculation of travel times, *Bull. Seismol. Soc. Am.* **78**, 2062–2076.
- Vidale, J. E. (1990). Finite-difference calculation of traveltimes in three dimensions, *Geophysics* **55**, 521–526.
- Wessel, P., and W. H. F. Smith (1998). New, improved version of the Generic Mapping Tools released, *Eos Trans. AGU* **79**, 579.

Department of Geophysics  
Kangwon National University  
1 Gangwondaehak-gil, Chuncheon-si  
Gangwon-do 200-701, South Korea  
sjchang@kangwon.ac.kr  
(S.-J.C.)

Department of Earth and Planetary Sciences  
Northwestern University  
Technological Institute  
2145 Sheridan Road  
Evanston, Illinois 60208-3130  
(S.V.)

Lawrence Livermore National Laboratory  
P.O. Box 808, L-205  
Livermore, California 94551  
(M.P.F.)